Fuel cell management system: An approach to increase its durability

Milad Bahrami, Jean-Philippe Martin, Gaël Maranzana, Serge Pierfederici, Mathieu Weber, Sophie Didierjean

Fuel cell management system: an approach to increase its durability

M. Bahrami[1*], J-P. Martin[1], G. Maranzana[1], S. Pierfederici[1], M. Weber[1], and S. Didierjean[1]
1- Université de Lorraine, CNRS, LEMTA, F-54000 Nancy, France

Abstract- The lifetime and cost are two bottlenecks in the widespread use of fuel cells. Increasing the lifetime of the fuel cell can also counteract the cost justification bottleneck. However, this depends on the method of extending the life of the fuel cell. The durability of Polymer Electrolyte Membrane Fuel Cells (PEMFCs) can be improved using a management system. This management system must control the operating condition of cells or cell groups in such a way that the electrochemical and fluidic instabilities can be avoided to improve the lifetime of a stack. Developing this Fuel Cell Management System (FCMS) is challenging due to the coupling between cells inside a stack. In this paper, an FCMS is proposed. It can detect the instability of cell groups and change their reference power based on the detected instabilities. Since a mathematical model has a high ability to describe the phenomena occurring in a fuel cell, this paper uses a model to describe its operating conditions. The reference power of the cell groups can be changed using a developed power electronics structure. The last piece of the FCMS puzzle is to develop a management strategy. This strategy is developed in this paper. Eventually, the proposed system is evaluated experimentally. The experimental results validate the effectiveness of the proposed system.

Keywords: Fuel cell management system, Polymer electrolyte membrane, Power electronics, Fuzzy logic control.

1. INTRODUCTION

Regarding the environmental problems of fossil fuels in electricity generation and the barriers in using renewable energy resources for any type of application, new ways in generating or storing electricity are inevitable [1–3]. The recent approach to Polymer Electrolyte Membrane Fuel cells (PEMFCs) proves this fact. However, cost and durability are two bottlenecks in the widespread use of this technology [4–6]. These barriers can be attributed to the used materials, low voltage of a cell, and the reaction products. Increasing the durability of PEMFCs can be done by replacing the used materials with cheaper and more durable materials or by using a Fuel Cell Management System (FCMS). The advantage of the FCMS is the possibility of using it for existing fuel cell systems [5,7–9].

1.1. Literature review

An online prognostic or diagnostic can be used to develop such a management system [7–10]. Generally, the prognostic or diagnostic methods can be divided into three groups: model-based, data-driven, and hybrid methods [9,11,12]. The major challenge in using the prognostic method is its need for vast Fuel Cell (FC) performance results under different operating conditions. The non-model-based diagnostic methods are divided into three groups: knowledge-based methods [13–15] signal-based methods [16], and hybrid methods [17]. The knowledge-based methods can be divided into two groups [11]: Artificial Intelligence methods [13,14], and statistical methods [15]. The non-model-based methods demand a database of different operational conditions to be trained. Therefore, these methods are time-consuming and they can cause irreversible damages to the faulty systems during the training time[11]. Due to a direct link between physical models and the FC phenomena, they can be very useful for developing a management system [18]. Besides, the model-based approach can provide degradation information about the internal physical parameters during the operation [19]. The models developed for FCs can be categorized into three groups: white-box [20], grey-box [21–23], and black-box [24–27]. The white-box models are the most complex ones and they are difficult to use in real-time whereas, the black-box models show a lack of genericity and are still for offline applications or they can be used to identify some of the fuel cell faults [27]. The grey-box models replace some of the complex equations in the white-box models with empirical equations or mapping tables. Some of the grey-box models can provide vast information on the FC phenomena in real-time.

In this direction, many efforts have been made in the literature to increase the durability of PEMFCs recently. In [28], the PEMFC performance was improved through a developed Energy Management System (EMS). The EMS shared the load power between the PEMFC and a Super Capacitor (SC) bank, taking into account the safe operating zone of the PEMFC. This zone was online estimated through an extremum-seeking method. In [29] a dynamic optimization strategy was proposed based on a proposed prognostication method of the remaining useful life of a solid oxide FC to minimize voltage degradation and maximize efficiency over the remaining useful life of the FC. An online energy management strategy based on a grey-box model and Kalman filter was proposed for a multi-stack FC to obtain maximum efficiency in [30]. This method led to more uniformity of degradation between the stacks. In [31], a control strategy based on multi-objective optimization and tracking the lower oxygen excess ratio was proposed to enhance the performance of a PEMFC. At the higher level of this method, the oxygen saturation and its conflict on the efficiency and maximum power were considered to evaluate the performance of the PEMFC. The lower level was for tracking the oxygen excess ratio to cope with the uncertainty of the PEMFC. The

system performance and its safety were improved by this method. In [32], the net output power of a PMFC through a sliding mode variable structure control was improved as an approach in improving its performance. A model was utilized to find a relation between the net output power with the temperature, fan power consumption, and load current. This method had better results compared to the conventional PID controller. In [33], an online nitrogen concentration observer was developed based on a mathematical model to improve the durability of a PEMFC through periodically purging anode. The experimental results proved the higher hydrogen utilization along with protecting the PEMFC. A diagnostic method based on wavelet transform of the stack voltage was developed in [34] that could identify different faults and their severities. They could distinguish different faults relating to the system auxiliaries but they didn't propose any approach to deal with the detected faults. In [35], a prognostic approach based on the recurrent neural network was developed for the PEMFC as an approach in output voltage degradation prediction. They claimed that this method will be used for developing health management in future work. Similarly, an artificial intelligence-based prognostic method was developed to estimate the remaining useful life of the PEMFC in [36], and it was claimed that this method will be used in future work to develop an energy and humidity management system. However, due to the learning procedure used in these methods, it will be time-consuming to develop such methods.

1.2. Problem statement and contribution

To improve the lifetime of a PEMFC, all of the aforementioned studies have considered it as a stack without considering its forming cells. The high number of cells inside a fuel cell stack can lead to different problems. The unsuitable assembly process of the stack can exacerbate the creep, material fatigue, the generation of cracks, and degradation of the seals [37]. For instance, the sealing degradation can lead to an increase in hydrogen crossover which is an indicator of fuel cell aging [38]. The large heterogeneity of the gas distribution between the cells inside a large stack is more conceivable [39]. Besides, the resistance of the cells in the middle of a stack may increase faster than the other cells [4] and due to the temperature misdistribution, the performance of the middle cells is lower than the side cells [4]. As a result, they could be at a different level of degradation. The cells inside a stack are electrically connected in series and thermally coupled. Therefore, the lifetime of a stack depends on the life of its cells. Due to the thermal coupling, the problem is more severe for a stack compared to a single cell. As seen in Fig. 1, the over-temperature of one cell related to its degradation level can influence the adjacent cells and create a temperature gradient for them. Since more water is evacuated from the colder side [40,41], more water is accumulated in the anode and cathode channels of the previous cell ($Cell_1$) and next cell ($Cell_3$) respectively. In this condition and since the cells inside a stack are under the same pressure drops inside their channels, the water can clog the channels and hydrogen starvation and oxygen starvation are quite conceivable for the previous and next cells respectively. Hence, a faulty cell can influence the whole stack. Hence, managing the whole stack has little impact on such phenomena. Since the flooding and drying conditions are the main reason for degradation [7], these two main causes of cell failure are considered as faults in this paper. The flooding condition can lead to fuel or oxygen starvation. The fuel starvation results in a higher potential of cathode and induced carbon corrosion that eventually leads to reduction of the electrode thickness and destroy the porous structure [42]. In [43], carbon corrosion was considered as the main reason for degradation as a consequence of fuel starvation because CO_2 was detected at the outlet of the cathode when a cell is under the condition of fuel starvation. In [4], it was proved by simulation that the amount of oxygen, which transfers to the anode in a cell under the fuel starvation condition, has a direct impact on the carbon corrosion rate [44]. The drying condition can lead to membrane rupture.

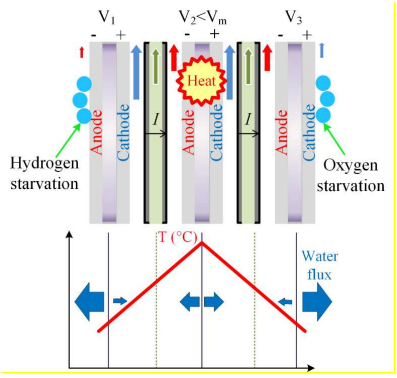

Fig. 1. Propagation of the instability of a single cell to its adjacent cells .

Using the concept of multi-stack management that can improve the cost and lifetime of the system [6], the main contribution of this paper is to develop an FCMS that changes the operating conditions of cell groups inside a stack according to their state to prevent them from moving toward an instability or fault. As a result, all cell groups will degrade together and the overall life of the stack will increase. Regarding this contribution, an online simple dynamical model that provides information about the cells inside a stack is required. This model was developed in our recent study [45]. . The required stack and power electronics structure were developed in [46] and [8] respectively. The last ring in the chain is the management strategy that should change the operating condition of cell groups based on the model results and using the power electronics structure is developed in this paper. A Fuzzy Logic Controller (FLC) based management system is the other contribution of this paper.

1.3. Paper organization

The rest of this paper is organized as follows: The management system is detailed in Section2. The proposed FLC controller is also explained in this section. The experimental results are provided and analyzed in Section 3. Finally, the conclusions are listed in Section 4.

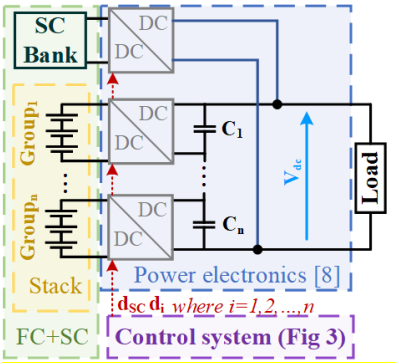

Fig. 2. Schematic diagram of the FCMS .

2. METHODOLOGY- SYSTEM CONFIGURATION

The schematic diagram of the system to implement the proposed FCMS is depicted in Fig. 2. As depicted in this figure, power electronics were developed in our recent study [8]. The control system part of this figure is shown in Fig. 3. As demonstrated in this diagram, the reference power of different cell groups inside a stack is adjusted by the management strategy which is the main contribution of this paper. The control loop, power electronics structure, and control system boxes in this figure were developed and explained in [7,8]. The real-time simulation model of PEMFC was developed in [45]. Based on the developed model, the instabilities of the cell groups inside one stack can be detected. The results of the proposed method must lead to commands which can drive the power electronics structure. The FC model is a grey-box model that couples the mass, heat, and charge transfer mechanisms. The input/output parameters of the model are shown in Fig. 4 along with the state variables. As seen in this figure, the voltage of the cell can be obtained as a function of its current and vice versa.

In addition to the current or voltage as input, the temperature of the adjacent cell groups, the cooling temperature at the anode and cathode side, the pressure drop inside the channels, the relative humidity at the anode channel inlet, and the concentration at the cathode channel inlet are the inputs of this model. Indeed, the voltage (or current) of a cell is calculated by the following equation in the proposed PEMFC model:

$$U_{cell} = \phi - R_{\Omega} I \tag{1}$$

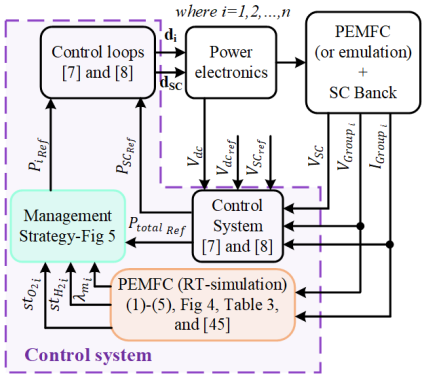

Fig. 3. Block diagram of the proposed control system.

where is U_{cell} is the voltage of a cell, I is its current, R is its ohmic resistance, and ϕ is its potential which can be calculated by considering the double layer effect as follows:

$$I_{C_{dl}} = -C_{dl}\frac{d\phi}{dt} \tag{2}$$

where C_{dl} is the double-layer capacity of the cell and $I_{C_{dl}}$ is the passing current through the double-layer capacitance of the cell which can be calculated by using the following equation:

$$I_{C_{dl}} = I - I^{f}_{H_2O\backslash O_2} \tag{3}$$

where $I^{f}_{H_2O\backslash O_2}$ is the faradic current which can be calculated from Butler-Volmer law [47]. This current requires the concentration of oxygen and water vapor inside the electrodes. The concentration of oxygen in the cathodic electrode ($C^{c,el}_{O_2}$) can be calculated based on its concentration inside the cathodic channel ($C^{c,ch}_{O_2}$) as follows:

$$C^{c,el}_{O_2} = C^{c,ch}_{O_2} - R^{diff}_{O_2}\frac{I}{4F} \tag{4}$$

where F is the faradic constant, I/4F is the oxygen consumption rate, and $R^{diff}_{O_2}$ is the oxygen diffusion resistance that its value depends on the cathodic compartment temperature. The thermal resistances along with three heat fluxes were used to calculate the temperature in the anode, cathode, and Membrane Electrode Assembly (MEA) as described in [41]. It should be noted that the thermal effect of the adjacent cells and cooling fluid were also modeled by thermal resistances. The heat flux in the MEA (ϕ_{MEA}), anode (ϕ^{th}_{a}), and cathode (ϕ^{th}_{c}) can be calculated as follows:

$$\begin{cases} \phi_{MEA} = \dfrac{I}{2F} LHV_{H_2} - U_{cell} I \\ \phi^{th}_{a} = Df_a L_v \\ \phi^{th}_{c} = Df_c L_v \end{cases} \tag{5}$$

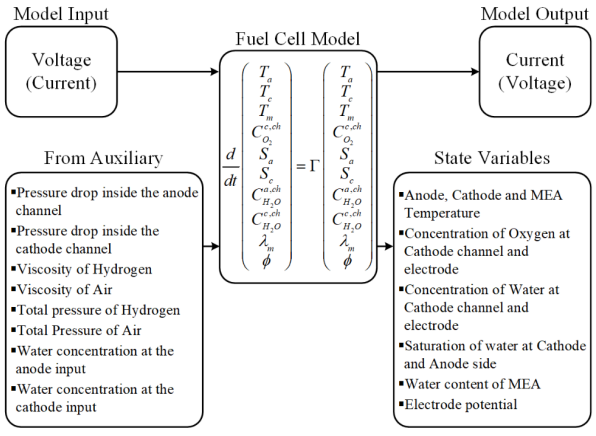

Fig. 4. Block diagram of the reduced-order transient PEMFC model.

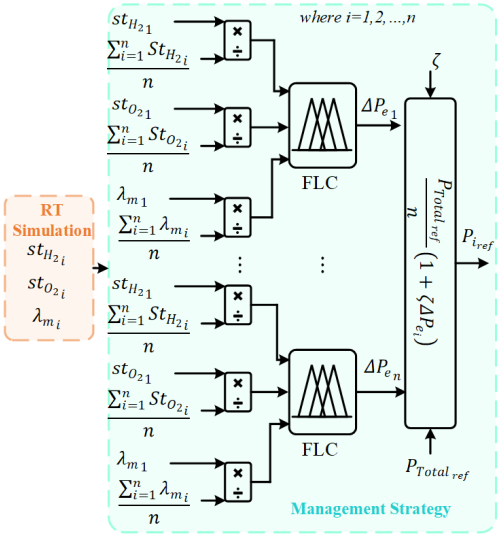

Fig. 5. Block diagram of the FCMS strategy.

where LHV_{H_2} is the lower heating value of Hydrogen (242 *kJ/mol*), *I/2F* is the Hydrogen consumption rate, L_v is the latent heat of the water (L_v=40.68 *kJ/mol*), and Df_a and Df_c are the water phase change flow rates in the anode and cathode channels. The heat and oxygen transfer models depend on the water transfer model. A diphasic flow-based water transfer model was developed and described in detail in [45] which was based on the Springer model [48]. It should be noted that the water transfer model has a relation with the heat transfer model. The proposed model can be used to emulate the behavior of a PEMFC. Using the current and voltage of the cell as the input of this model can make it stronger for estimating the state variables. Therefore, the proposed model with measuring voltage and current is used as the PEMFC RT-Simulation part of Fig. 3. Since the pressure drop is imposed in this model, it can simulate the behavior of a single cell inside its stack environment. Based on this model and given the pressure drops inside the channels, the Hydrogen flow rate ($N_{H_2}^{in}$) and airflow rate N_{air}^{in} at the inlet of the channels can be calculated and as a result the stoichiometry of Hydrogen (St_{H_2}) and Oxygen (St_{O_2})as follows:

$$\begin{cases} St_{H_2} = \dfrac{N_{H_2}^{in}}{I/2F} \\ St_{O_2} = \dfrac{0.21 N_{air}^{in}}{I/4F} \end{cases} \tag{6}$$

The idea of cell instability detection is to trace some parameters of the PEMFC model. The deviation of these parameters from their average values between the cell groups can be interpreted as different instabilities. Then, the desired decisions are taken and the power injected by the cell groups is adjusted to cure the defected cell groups. Three model parameters (stoichiometry of Hydrogen (St_{H2}), the stoichiometry of Oxygen (St_{O2}), and the water content of the membrane (λ_m)) have a link to the drying and flooding conditions are used to detect the cell instabilities. The water content is the number of water molecules in the active site of (SO_3^-). Reducing this parameter can be an indicator of drying. However, this parameter is not useful to detect the gas starvation problems that originated from the flooding conditions of cell groups. The origin of the gas starvation is inside the gas channels. As a result, the stoichiometry of Oxygen and Hydrogen is used to detect the flooding condition of cell groups and to distinguish which part of the cell was drowned. The main reason for choosing these two parameters is their direct relation with the liquid water level inside the anode and cathode channels. Because of the strongly nonlinear relationship of these parameters with the corresponding phenomena and the value of injected power by cell groups, FLC with a lower level of complexity is utilized to change the cell operating conditions based on selected parameters. Robustness, fast performance, and design simplicity are among the most important advantages of this method [2].

The block diagram of the management strategy is depicted in Fig. 5. As seen in this figure, the three model parameters from the RT-simulation are normalized by their average value between cell groups. These normalized values are the inputs of the FLC. The normalized value of the injected electrical power change by different cell groups (ΔP_{e_i}) is the output of the FLC. The total power supplied by different cell groups must be equal to the demanded total reference power by the SC bank controller in the steady-state. However, each group of cells has its FLC and ΔP_e and as a result, the sum of reference powers is not necessarily equal to the demanded total reference power by the SC controller. Therefore the last part of this management approach assures that the total power supplied by cell groups to be equal to the total reference power ($P_{Total_{ref}}$) in steady-state imposed by the SC voltage control loop while considering the maximum injectable power of cell groups. As seen in this figure, ζ is used to limit the maximum amount of injected power change. This parameter has a value between zero and one. In other words, $P_{Total_{ref}}/n$ (where n is the number of cell groups) and ζ are used to convert the normalized value of electrical power change to an absolute value. The reference powers ($P_{i_{ref}}$) is controlled by the control loops explained in [8]. The FLC should be slow enough (slower than the control loops i.e. the SC voltage controller) to respect the dynamic of the PEMFC and to not impact the SC voltage controller. This strategy sees the electrical power modifications as an external perturbation and can reject its impact on the total power which must be injected by the cell groups to stabilize the voltage of the SC in the steady-state.

A. FLC

The FLC method consists of four main parts: 1) fuzzification, 2) rule-based reasoning, 3) inference and 4) defuzzification. The FLC inputs turn to fuzzy language in the fuzzification part. Then the outputs in the inference section are made based on the laws in the rule-base. In the Defuzzification part, quantifiable

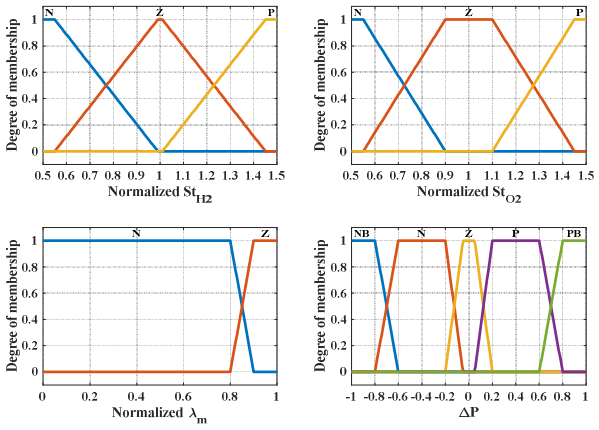

Fig. 6. Membership functions: inputs (St_{H_2} , St_{O_2} , and λ_m) and output (ΔP_e).

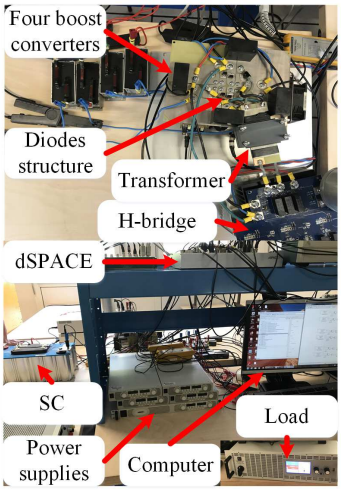

Fig. 7. Test bench of the proposed system.

results are produced from the outputs of the inference part [2]. Mamdani-type FLC consists of five steps: Fuzzification, apply fuzzy operator, apply the implication method, apply the aggregation method, and defuzzification [49].

The membership functions of the inputs and output of the FLC are shown in Fig. 6. Mamdani fuzzy inference system is used to implement the FLC. For the sake of simplicity, the number of membership functions for each input and output was tried to be as low as possible. These functions and their intervals were obtained through a trial and error procedure in which the following equation was tried to be minimized:

$$Error = \frac{1}{3n}\sqrt{\sum_{i=1}^{n}\left(1-\lambda_{m_i}\right)^2+\left(1-St_{H_{2_i}}\right)^2+\left(1-St_{O_{2_i}}\right)^2} \qquad (7)$$

Through this trial and error procedure, different membership functions with different intervals were utilized. However, the rule base was the same for all of them. For each one, the simulation was iterated for the normal, drying, and flooding conditions of the first cell group while the other groups were in normal condition. The utilized membership functions with the minimum oscillation results during the transient condition were compared by their static error based on (7) and the best one was adopted.

The universe of discourse for the inputs and output of the FLC is shown in Table 1. This table was adjusted relying on the expert information and based on the experiences that were conducted in LEMTA Laboratory. As seen in Table 1, the electrical power change is primarily affected by the normalized value of the water content when this value is less than one. The next priority in changing the injected power of the cell belongs to the normalized value of Hydrogen stoichiometry. These priorities were adopted based on their impact on cell degradation [50]. More precisely, the Negative (N) water content means the cell is about to be dried (or is already dried) and thus the power should be increased to produce more water (to reduce the cell stoichiometry). However, the magnitude of this change depends on the two other inputs of the FLC. The Negative (N) stoichiometry means that a high amount of liquid water appeared in the channels and therefore, the power should be decreased to produce less water (to increase the stoichiometry). Conversely, the Positive (P) Stoichiometry means that the cell is about to be dried. The electrical power of the cell should be increased to reduce the stoichiometry when the stoichiometry is Positive. The Zero (Z) state of the inputs means that they have a normal value and as a result, the supplied power should not be changed (Z or Zero) in this case. For instance, the change in the output power is Positive Big (PB) when the water content is Negative (N) and one of the

Table 1. Rule base of the fuzzy logic controller

RULE NO.	If St_{H2}	& If St_{O2}	& If λ_m	Then ΔP_e	RULE NO.	If St_{H2}	& If St_{O2}	& If λ_m	Then ΔP_e
1	Z	Z	Z	Z	10	Z	Z	N	PB
2	P	Z	Z	PS	11	P	Z	N	PB
3	N	Z	Z	NS	12	N	Z	N	PS
4	Z	N	Z	NS	13	Z	N	N	PS
5	P	N	Z	Z	14	P	N	N	PB
6	N	N	Z	NB	15	N	N	N	PS
7	Z	P	Z	PS	16	Z	P	N	PB
8	P	P	Z	PB	17	P	P	N	PB
9	N	P	Z	Z	18	N	P	N	PS

Table 2. Control parameters.

Parameter	Unit	Value
ζ	-	0.3
$\omega_{f_{Iref}}$	*Rad/s*	2π
K_P	-	0.1
K_{SC}	*Rad/s*	0.2π
KI_{SC}	Rad^2/s^2	0.01
$\omega_{f_{Vsc}}$	*Rad/s*	0.1π

stoichiometries or both of them are Positive (P). The output power change is kept PB even when the oxygen stoichiometry is Negative (N) and two other inputs are Positive (P) due to the priority of the water content and hydrogen stoichiometry. Due to considered priorities, the output power change is Positive Small (PS) when the stoichiometry of hydrogen and oxygen are respectively Negative (N) and Positive and the water content is Negative (N). Notably, a separate FLC with the same features is used for each group of cells, and the FLC runes every 100 s.

3. RESULTS AND DISCUSSION

To validate the proposed FCMS, a testbench was developed in LEMTA Laboratory. As seen in Fig. 7, four programable power supplies were used to emulate cell groups based on the proposed model but with just measuring the current of the cell and obtaining its voltage based on (1) to control the output voltage of programmable power supplies. It should be noticed that The cell groups are not thermally connected (to each other) for the sake of simplicity in result assessment. The temperature of the adjacent cells for each group of cells is equal to 60 °C. The first group is considered the defective group. Each group

Table 3. Parameters of the FC model.

Parameter	Value	Unit	description	Parameter	Value	Unit	description
L	0.3	m	Length of the active area	$e_{c,ch}$	0.29	mm	Cathode channel depth
W	0.01	m	Width of the active area	$e_{a,ch}$	0.12	mm	Anode channel depth
e_{GDL}	2.5×10^{-4}	m	Thickness of the GDL	ρ_{dry}	2020	kg/m^3	Volumetric mass of the dry membrane
λ_{GDL}	0.3	$W/m°K$	Effective thermal conductivity of GDL	EW	1.1	kg/mol	Equivalent weight of the membrane
ρ_{MEA}	2020	kg/m^3	Volumetric mass density of MEA	ξ	0.45	-	Electro-osmosis coefficient
C_{MEA}	1000	$J/kg°K$	Specific heat capacity of MEA	R_e	20	$m\Omega.cm^2$	Electrical resistance of the cell
e_{MEA}	5×10^{-5}	m	Thickness of the MEA	C_{dl}	0.2	F/cm^2	Double-layer capacity of the cell
D_m	6×10^{-6}	m^2/s	water diffusion coefficient through the membrane without the temperature effect	γ	200	-	Roughness factor of the electrode
$D_{H_2O}^{a,GDL}$	2.5×10^{-5}	m^2/s	Water diffusion coefficient through the anodic GDL without the temperature effect	$I_0^{H_2O\backslash O_2}$	0.05	A/m^2	Exchange current density
$D_{H_2O}^{c,GDL}$	1.2×10^{-5}	m^2/s	Water diffusion coefficient through the cathodic GDL without the temperature effect	$E_{H_2O\backslash O_2}^{ref}$	0.95	V	Standard cell potential
$D_{O_2}^{0,GDL}$	1.2×10^{-5}	m^2/s	Oxygen diffusion coefficient at temperature T0	$\alpha_{H_2O\backslash O_2}^{ox,Pt}$	1	-	Anodic charge transfer coefficient
ρ_p	2000	kg/m^3	Volumetric mass density of the plate	$\alpha_{H_2O\backslash O_2}^{red,Pt}$	1	-	Cathodic charge transfer coefficient
C_p	7200	$J/kg°K$	Specific heat capacity of plate	k_g^a	2.87×10^{-15}	m^3	Model parameter
e_p	2×10^{-3}	m		k_g^c	3×10^{-14}	m^3	Model parameter
R_f^{th}	$R_{GDL}^{th}/10$	W/°C	Thermal resistance with the cooling fluid	$k_{liq}^a = k_g^a$ $k_{liq}^c = k_g^c$	2.87×10^{-15} 3×10^{-14}	m^3	Model parameter
R_c^{th}	$R_{GDL}^{th}/10$	W/°C	Thermal resistance with the adjacent cells	α	3	-	Model constant

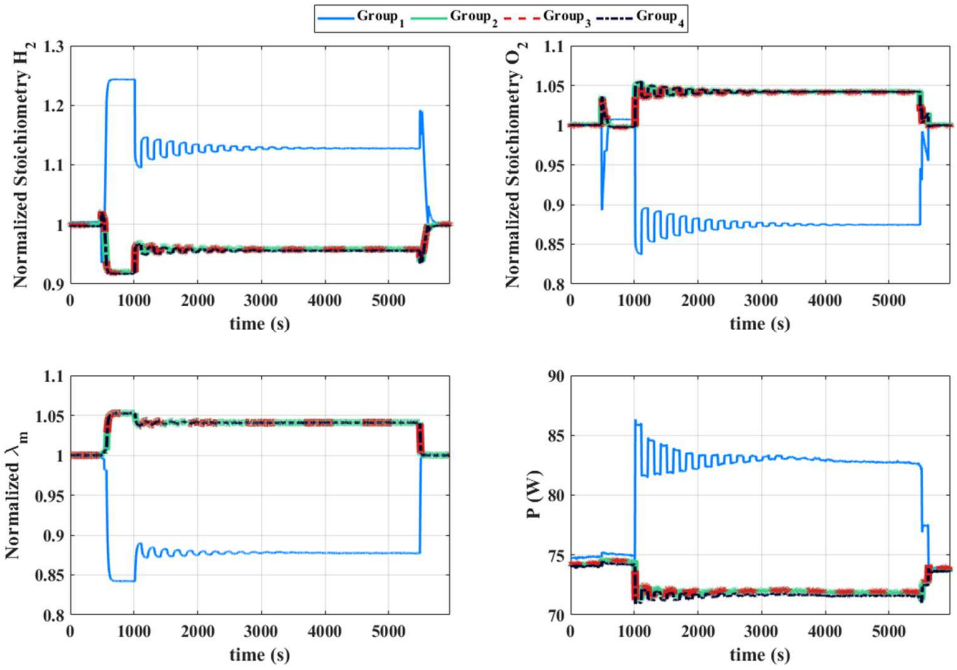

Fig. 8. Experimental results of the normalized value of the FLC inputs and the reference power that should be injected by the cell groups when the cooling fluid temperatures of the first group increased from 60 ºC to 75 ºC at 1000 s and decreased to its nominal value of 60 ºC at 5500 s (The air and hydrogen pressure drops are applied).

consists of seven cells that are connected in series. The control parameters are shown in Table 2. To control the programable power supply and the power electronic structure, and to realize the FCMS, the dSPACE 1005 was used. Besides, a constant resistive load was used in this testbench. It should be noted that the temperature, flow rates, saturation levels, and cell voltages are obtained from the models which emulate the cell groups by using the programmable power supplies. The other results are obtained from the model (by measuring the voltage and current) which is used as a part of FCMS.

To verify and validate the proposed FCMS, two experiments are performed. In these experiments, all of the four cell groups are in the normal condition until 500 s. The boundary conditions of the first group are changed at 500 s to simulate a fault. It should be declared that the boundary condition of the first cell is just changed in the model which was used to emulate the first cell group and control the programmable power supply.

In the first experiment, the drying condition of the first group is emulated by increasing the cooling fluid temperatures of the first group. A step of 15 degrees of Celsius increases the cooling fluid temperatures from 60 °C to 75 °C at 500 s and the same step decreases the temperatures from 75 °C to 60 °C at 5500 s. The applied pressure drop in the anode and cathode channels of cells is equal to 4000 Pa. The dew point temperature at the cathode and anode inlets are applied with bubblers at 46°C (anode side) and 52°C (cathode side). In this experiment, the FCMS runs after 1000 s. The current passing through the cell groups is fixed to be around 15 A in the normal condition of the cell groups by applying an appropriate load power. The PEMFC model parameters are shown in Table 3. The other model parameters and the boundary conditions are kept the same as [45].

The normalized and absolute values of the FLC inputs are respectively shown in Fig. 8 and Fig. 9. As seen in these figures, the FCMS runs after 1000 s and can improve the state of the first group. The inputs of the FLC and the reference of powers in a steady state without utilizing the FCMS are compared to their values in steady-state with utilizing the FCMS in Table 4 based on Fig. 8 and Fig. 9. In this table, the relative error for each parameter can be calculated by (8). This table shows that a 4% modification of water content dispersion is obtained at a cost of increasing the power dispersion by 12%.

$$\mathrm{Re}_x = \frac{abs(x_1 - x_{other\ groups})}{\max\left(x_1, x_{other\ groups}\right)} \tag{8}$$

In this equation, Re_x is the relative error of the x (x can be the membrane water content, hydrogen stoichiometry, oxygen stoichiometry, or injected power) and the index of x indicates the cell group.

The temperature of the cell groups is shown in Fig. 10. The appearance or disappearance of liquid water takes time. Therefore, the stoichiometry of hydrogen and oxygen has a transient state when the temperature of the cooling fluids is changed. The temperature rise influences gas viscosity and water vapor flow rate before changing the amount of liquid water. As a result, the stoichiometry of the gases is primarily decreased due to the viscosity changes and the increase of the water vapor flow rate. Then, it increased due to the disappearance of the liquid water from the channels. As shown in Fig. 11, the dry gas flow and the saturation level inside the channels verify this theory. The same reason is behind the

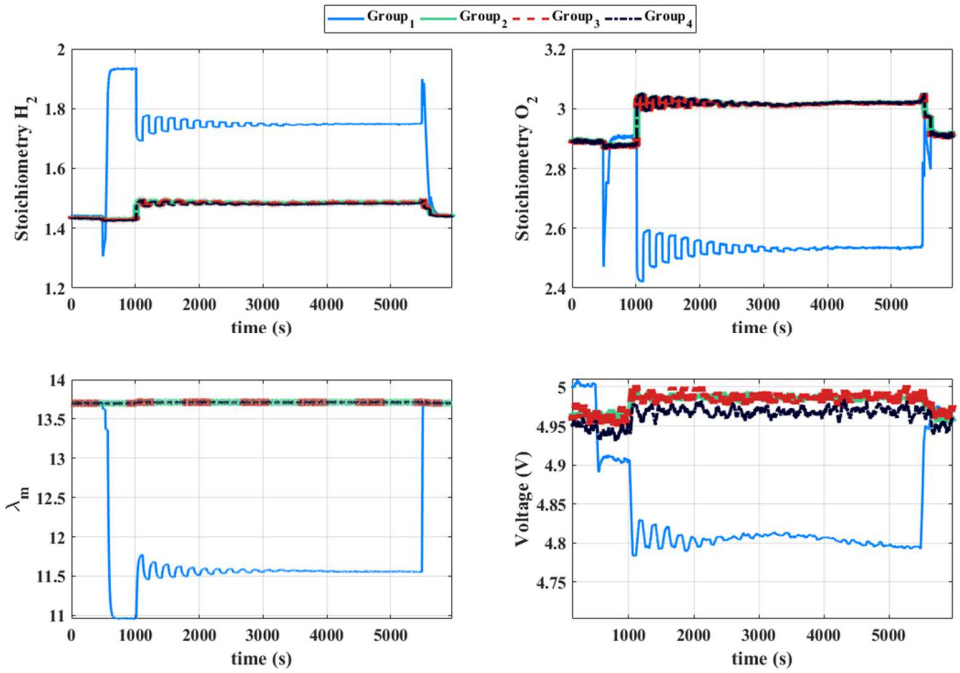

Fig. 9. Experimental results of the FLC inputs and the cell voltages when the cooling fluid temperatures of the first group increased from 60 ºC to 75 ºC at 1000 s and decreased to 60 ºC its nominal value at 5500 s (The air and hydrogen pressure drops are applied).

increase of stoichiometry when the cooling fluid temperatures return to their nominal value at 5500 s. As seen in Fig. 11, the saturation levels increased from zero to their nominal value at 5500 s. As a result, the dry gas flow rates primarily increased due to the change of viscosity and water vapor flow rate. Then, it decreased to its nominal value due to the saturation level change.

Briefly, due to the temperature rise at 500 s (Fig. 10), the water saturation in the anode and cathode sides of the first group decreases to zero (Fig. 11). This lower saturation level

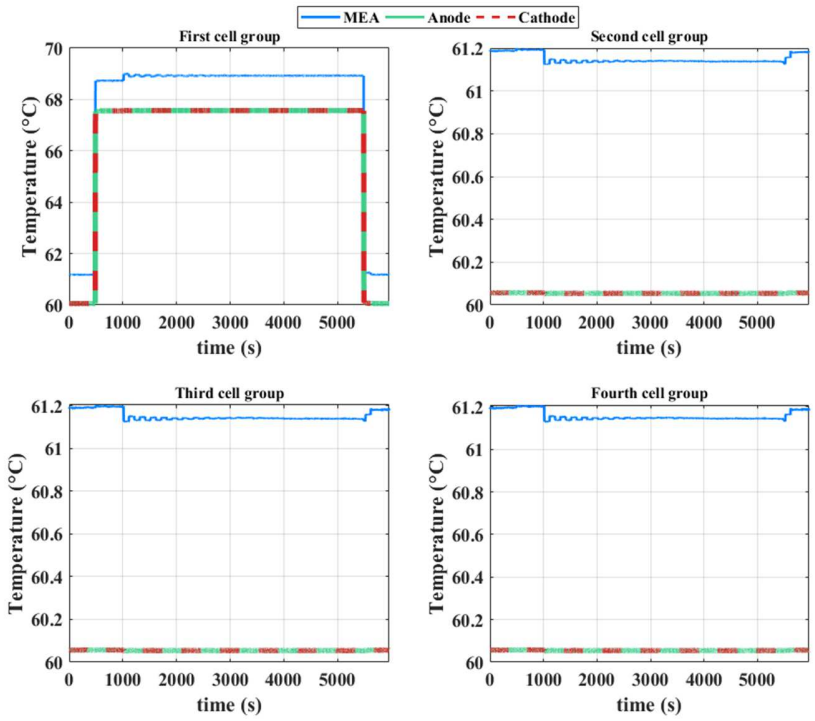

Fig. 10. Experimental results of the cell temperatures when the cooling fluid temperatures of the first group increased from 60 ºC to 75 ºC at 1000 s and decreased to 60 ºC its nominal value at 5500 s (The air and hydrogen pressure drops are applied).

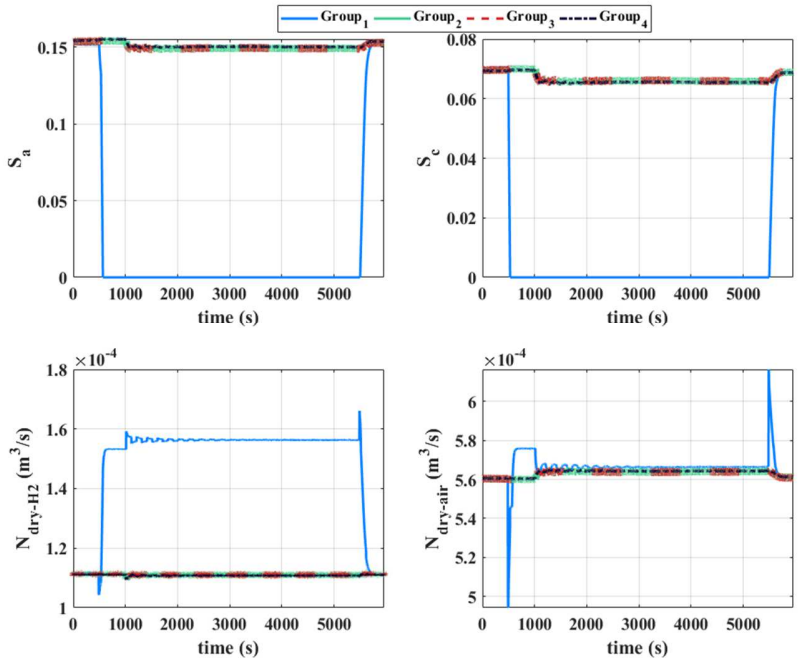

Fig. 11. Experimental results of the saturation level inside the channels and dry gas flow rates when the cooling fluid temperatures of the first group increased from 60 ºC to 75 ºC at 1000 s and decreased to 60 ºC its nominal value at 5500 s (The air and hydrogen pressure drops are applied).

leads to the gas flow rate increase (Fig. 11). Therefore, the stoichiometry of hydrogen and oxygen increased as shown in Fig. 9. The gas flow rates and consequently the stoichiometries are initially reduced due to the delay in the disappearance of the water droplets. The decrease in the flow rates is due to the viscosity change due to temperature change and the change of the vapor water flow rate. Then, the water droplets disappear and as a result, the flow rates decreased. The membrane water content of the first group is also depicted in Fig. 9. The water content decreased due to the cooling fluid temperature rises. This reduction makes the membrane more resistive and as a result, the cell voltage of the first group decreased (Fig. 9). This condition is the drying condition. The FCMS consequently increases the electrical power injected by the first group to produce more water. It should be noted that decreasing the local stoichiometry can also deal with this issue. However, this power rise leads to reducing the stoichiometry of hydrogen and oxygen. Because of this drastic reduction of the oxygen stoichiometry, the FCMS slightly reduces the injected power by the first group. To keep all three inputs of the FLC at the closest possible value to one, the FCMS has reached the final value of injected powers by the cell groups after some oscillations in transient conditions.

The demanded total reference power by the SC controller ($P_{Totalref}$) and the total supplied power ($P_{Total} = \sum_{i=1}^{4} P_{i_{ref}}$) is shown in Fig. 12 during this experiment. Since the FCMS runs

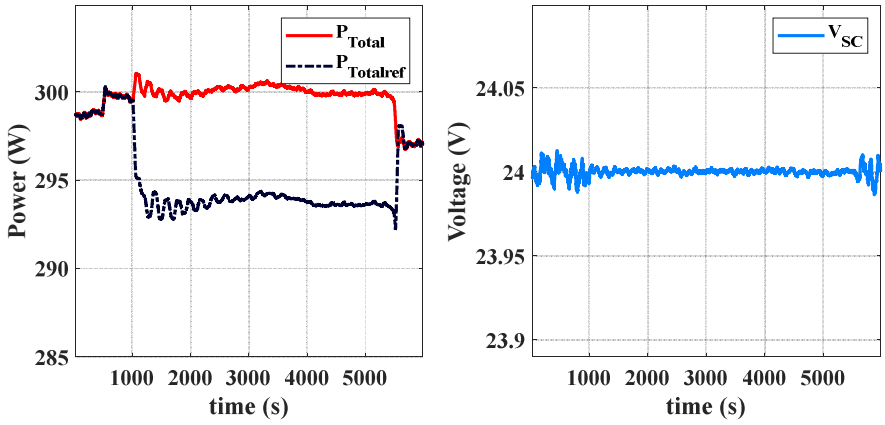

Fig. 12. Experimental results of the SC voltage, the reference of total power, and the total power injected by cell groups when the cooling fluid temperatures of the first group increased from 60 ºC to 75 ºC at 1000 s and decreased to 60 ºC its nominal value at 5500 s (The air and hydrogen pressure drops are applied).

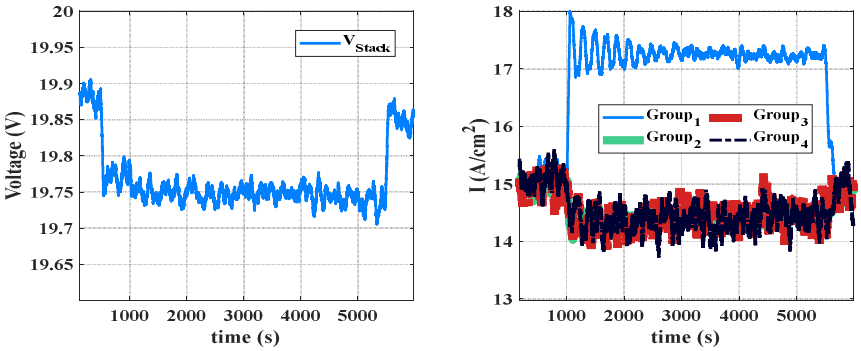

Fig. 13. Experimental results of the stack voltage and the injected current by cell groups when the cooling fluid temperatures of the first group increased from 60 ºC to 75 ºC at 1000 s and decreased to 60 ºC its nominal value at 5500 s (The air and hydrogen pressure drops are applied).

after 1000 s, a difference appears between these powers. As seen in Fig. 8, the first power is increased by the FCMS by changing the ΔP_{e_1}. In this case, if the $P_{Totalref}$ stays constant, the P_{Total} would be higher than the load power. Therefore, the SC controller reduced $P_{Totalref}$ to have constant power at the output related to the load power ($P_{Total} = P_{load}$). The SC voltage is also changed during the transient conditions to regulate the DC link voltage but it cannot be seen because of the used time scale. The stack voltage is shown in Fig. 13. As seen in this figure, the stack voltage is decreased (19.9 V to 19.75) due to the drying condition of the first group but the stack voltage remains the same after running the FCMS. This result further verifies the effectiveness of the proposed FCMS. The current density of cell groups is also shown in Fig. 13 that is changed due to the FCMS and the SC voltage controller. The higher current density of the first group is coherent with its higher power (Fig. 8). This higher current density means more water production to deal with the drying condition of the first group.

The second experiment stands for simulating the flooding condition of the first group. A step of 5 degrees of Celsius increases the cathode side cooling fluid temperature of the first group from 60 °C to 65 °C at 500 s (just in the CM). The same step is used to decrease it from 65 °C to 60 °C at 4500 s. In this experiment, the applied pressure drop in the anode and cathode channels of cells is equal to 4000 Pa and 3800 Pa respectively. The dew point temperature at the cathode and anode inlets are applied with bubblers at 60°C (cathode and anode). The model parameters are the same as in Table 3. The FCMS runs after 1000 s.

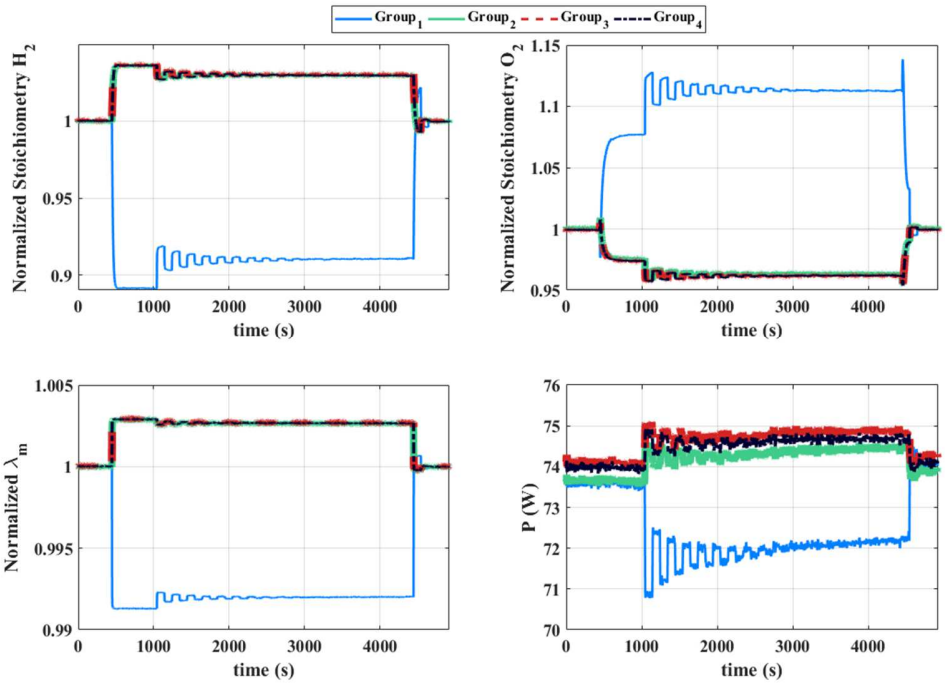

Fig. 14. Experimental results of the normalized value of FLC inputs and the reference power that must be injected by the cell groups when the cathode side cooling fluid temperature of the first group increased from 60 ºC to 65 ºC at 1000 s and decreased to its nominal value of 60 ºC at 4500 s (The air and hydrogen pressure drops are applied).

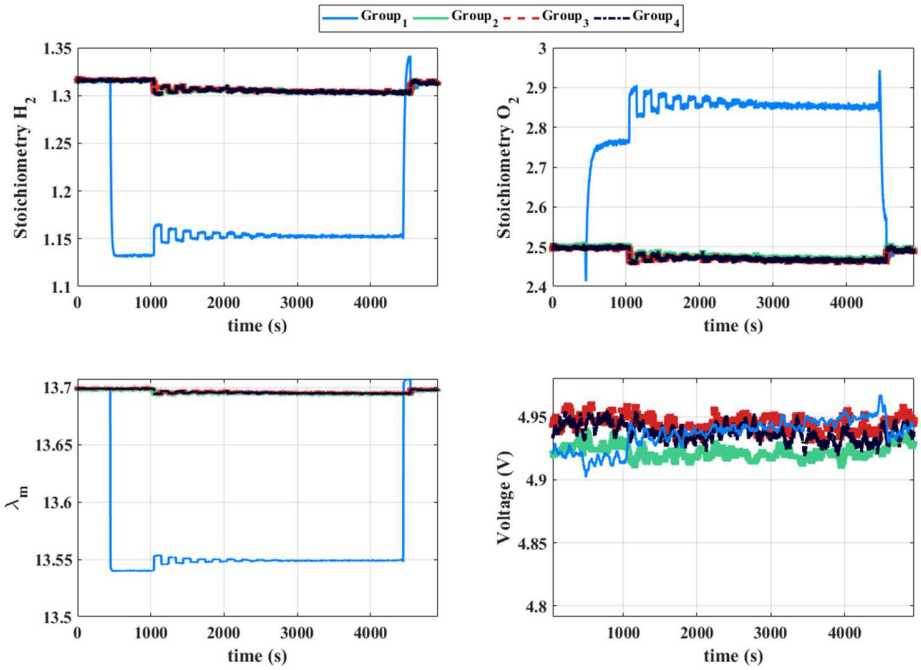

Fig. 15. Experimental results of FLC inputs and the cell voltages when the cathode side cooling fluid temperature of the first group increased from 60 ºC to 65 ºC at 1000 s and decreased to its nominal value of 60 ºC at 4500 s (The air and hydrogen pressure drops are applied).

The normalized and absolute values of the FLC inputs are respectively shown in Fig. 14 and Fig. 15. As seen in these figures, the FCMS improves the state of the first group after it runs at 1000 s.

The inputs of the FLC and the reference of powers in the steady-state without utilizing the FCMS are compared to their values in steady-state in the presence of the FCMS in Table 5 based on Fig. 14 and Fig. 15. This table shows that a 3% modification of the hydrogen stoichiometry dispersion requires increasing the power dispersion by 3%.

The experimental results of the cell group temperatures are shown in Fig. 16 for the second experiment. The cathode side

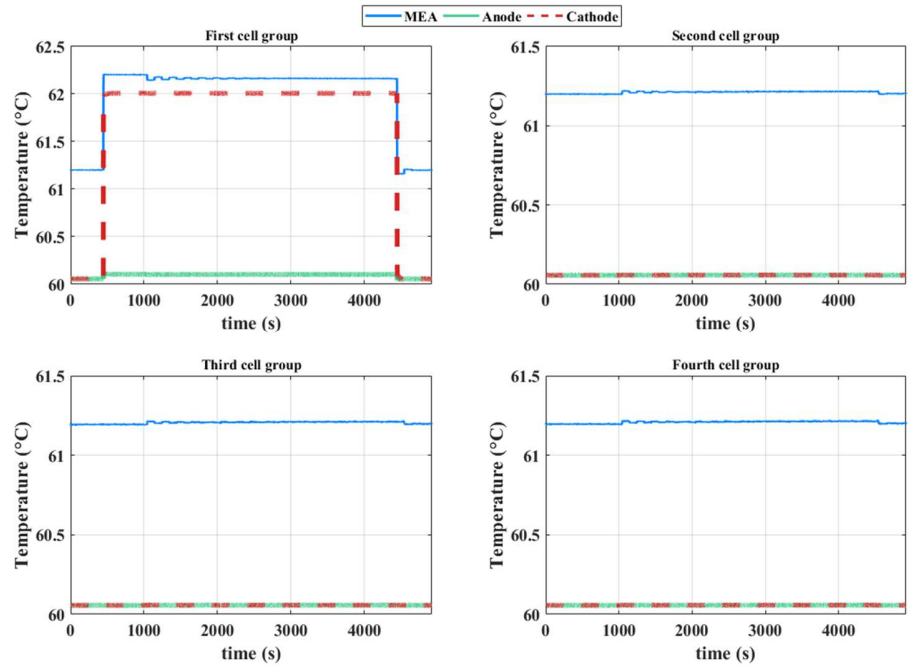

Fig. 16. Experimental results of the cell temperatures when the cathode side cooling fluid temperature of the first group increased from 60 ºC to 65 ºC at 1000 s and decreased to its nominal value of 60 ºC at 4500 s (The air and hydrogen pressure drops are applied).

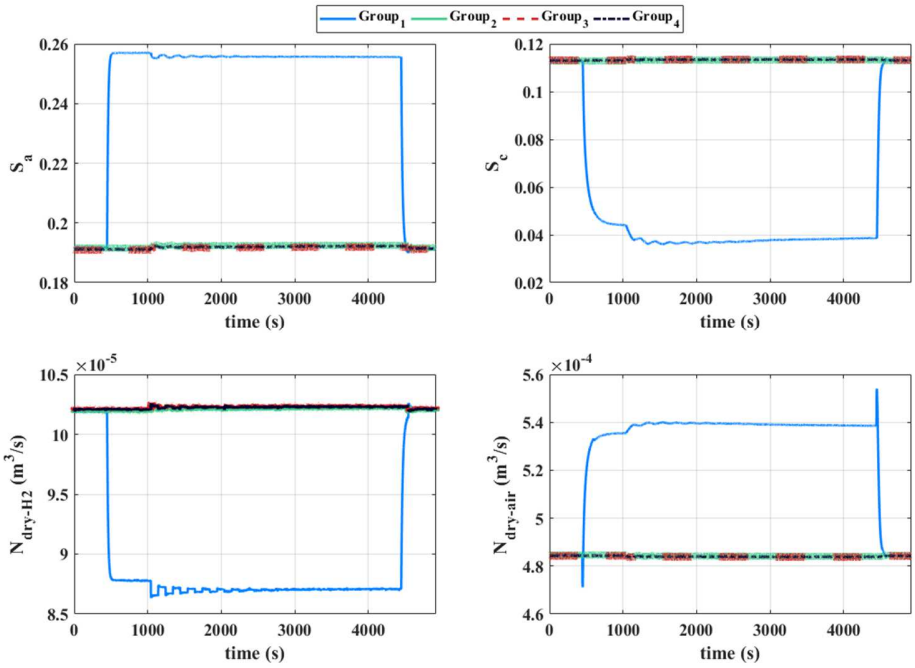

Fig. 17. Experimental results of the dry gas flow rate and saturation inside the channels when the cathode side cooling fluid temperature of the first group increased from 60 ºC to 65 ºC at 1000 s and decreased to its nominal value of 60 ºC at 4500 s (The air and hydrogen pressure drops are applied).

cooling fluid temperature increase leads to a temperature gradient between anode and cathode of the first group of cells. Due to this temperature gradient between the anode and cathode of the first group at 500 s, more water is accumulated in the anode side of the first group and the level of saturation in its anode channel is increased (Fig. 17). As a result, the hydrogen flow rate decreased and the hydrogen stoichiometry of the first group consequently decreased after applying the rise in the cathode side cooling fluid temperature of the first group at 500 s. Due to the water transfer to the anode side, the water vapor flow rate at the cathode decreased and consequently, the oxygen stoichiometry increased (Fig. 17). However, due to the more water accumulation in the anode side, the hydrogen flow rate drops, and the hydrogen stoichiometry of the first group consequently decreased. This lower value of hydrogen stoichiometry is an indicator of fuel starvation.

The FCMS (after 1000 s) decreases the injected power of the first group to struggle with the hydrogen stoichiometry reduction. However, the stoichiometry of oxygen is increased due to this power reduction. Regarding the intervals of the membership functions, which are adjusted for the FLC inputs, the power of cell groups is stabilized after a bit of oscillation.

The P_{Total} and $P_{Totalref}$ is shown in Fig. 18 during the second experiment. Since the FCMS runs after 1000 s, the $P_{Totalref}$ is a bit different from the P_{Total} due to the disturbance created by the FCMS. As described for Fig. 12, the $P_{Totalref}$ is changed to

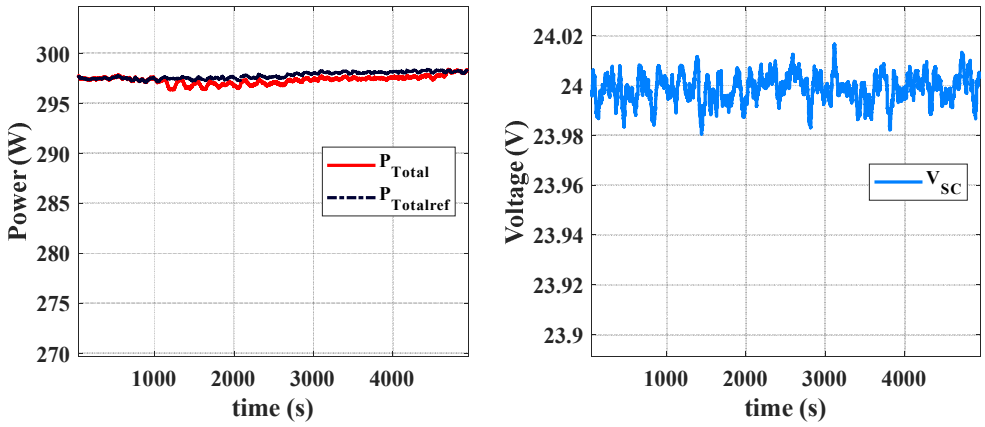

Fig. 18. Experimental results of the SC voltage, the reference of total power, and the total power injected by cell groups when the cathode side cooling fluid temperature of the first group increased from 60 ºC to 65 ºC at 1000 s and decreased to its nominal value of 60 ºC at 4500 s (The air and hydrogen pressure drops are applied).

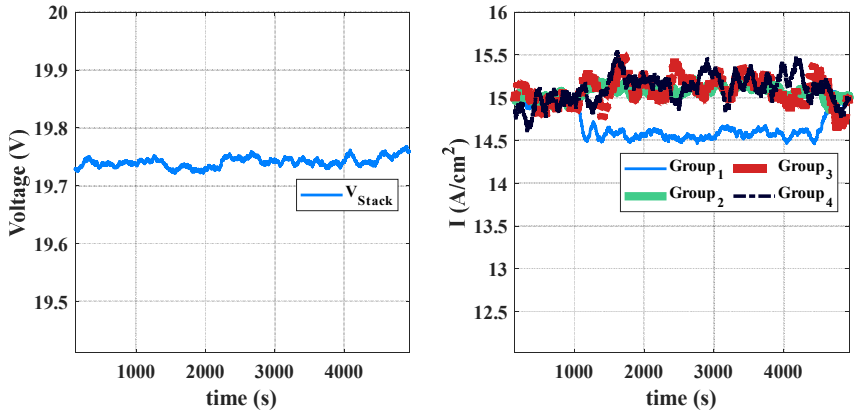

Fig. 19. Experimental results of the stack voltage and the injected current by cell groups when the cathode side cooling fluid temperature of the first group increased from 60 ºC to 65 ºC at 1000 s and decreased to its nominal value of 60 ºC at 4500 s (The air and hydrogen pressure drops are applied).

have constant power at the output related to the load power ($P_{Total} = P_{load}$).As depicted in Fig. 18, the SC voltage is constant in steady-state. As seen in Fig. 19, the stack voltage is very slightly changed. As seen in Fig. 15, the most important objective, in this case, was to guarantee the hydrogen supply to avoid hydrogen starvation. The current density of cell groups is also shown in Fig. 19 that is changed due to the FCMS, the SC voltage controller, and the loop between the reference power and the output voltage of the cell. The lower current density of the first group is coherent with its higher power (Fig. 14). This lower current density means lower water production to deal with the flooding condition of the first group.

These two experiments validate the effectiveness of the proposed FCMS during the transient condition and verify that this system can return the electrical current to its nominal values once the fault was solved.

4. CONCLUSION

A management strategy was developed in this paper for PEMFCs. This management system can deal with the instabilities of cells inside a stack or the instability of a stack in a multi-stack system. Indeed, using the information provided by the FC model and based on a proposed FLC, the operating condition of the cell groups is changed by the proposed system to deal with their faults. The drying and flooding (fuel starvation) conditions as the most important instabilities of the cell were experimentally assessed by the proposed system. The experimental results, which were provided in this paper, verify the capability of the proposed system. Based on the experimental results, the FCMS could improve the operational condition of the first cell group (as a defective group), by changing its injected power. As a result, the FCMS could prevent the first group from fuel starvation and drying condition. In this way, the total lifetime of the system can be improved by preventing instabilities and even by putting the defective group out of connection in the worst condition.

Table 4. Inputs of the FLC and reference of powers in the steady-state during the drying condition of the first group

	λ_m	St_{H_2}	St_{O_2}	Power
First group- without the FCMS	10.96	1.93	2.9	75.02
The other groups (average value)– without the FCMS	13.7	1.43	2.88	74.5
Relative error- without the FCMS	0.2	0.26	0.01	0.01
First group- with the FCMS	11.56	1.75	2.53	82.63

5. REFERENCES

[1] Zandi M, Bahrami M, Eslami S, Gavagsaz-Ghoachani R, Payman A, Phattanasak M, et al. Evaluation and comparison of economic policies to increase distributed generation capacity in the Iranian household consumption sector using photovoltaic systems and RETScreen software. Renew Energy 2017;107:215–22.

[2] Bahrami M, Gavagsaz-Ghoachani R, Zandi M, Phattanasak M, Maranzanaa G, Nahid-Mobarakeh B, et al. Hybrid maximum power point tracking algorithm with improved dynamic performance. Renew Energy 2019;130:982–91. https://doi.org/10.1016/j.renene.2018.07.020.

[3] Song K, Wang X, Li F, Sorrentino M, Zheng B. Pontryagin's minimum principle-based real-time energy management strategy for fuel cell hybrid electric vehicle considering both fuel economy and power source durability. Energy 2020;205:118064. https://doi.org/10.1016/j.energy.2020.118064.

[4] Hu Z, Xu L, Li J, Gan Q, Xu X, Song Z, et al. A novel diagnostic

Table 5. Inputs of the FLC and reference of powers in the steady-state during the flooding condition of the first group

	λ_m	St_{H_2}	St_{O_2}	Power
First group- without the FCMS	13.54	1.13	2.76	73.54
The other groups (average value)– without the FCMS	13.7	1.31	2.5	73.9
Relative error- without the FCMS	0.01	0.14	0.09	0
First group- with the FCMS	13.55	1.15	2.84	72.15
The other groups (average value)– with the FCMS	13.69	1.3	2.46	74.66
Relative error- with the FCMS	0.01	0.11	0.13	0.03

methodology for fuel cell stack health: Performance, consistency and uniformity. Energy Convers Manag 2019;185:611–21. https://doi.org/10.1016/j.enconman.2019.02.031.

[5] Huang Z, Zhao J, Jian Q. Voltage behavior improvement for proton exchange membrane fuel cell stack suffering fuel starvation. Energy Sources, Part A Recover Util Environ Eff 2019;00:1–15. https://doi.org/10.1080/15567036.2019.1674962.

[6] Jahromi MM, Heidary H. Durability and economics investigations on triple stack configuration and its power management strategy for fuel cell vehicles. Int J Hydrogen Energy 2021;46:5740–55. https://doi.org/10.1016/j.ijhydene.2020.11.103.

[7] Bahrami M, Martin J, Maranzana G, Pierfederici S. Multi-Stack Lifetime Improvement through Adapted Power Electronic Architecture in a Fuel Cell Hybrid System. Mathematics 2020;8:739. https://doi.org/10.3390/math8050739.

[8] Bahrami M, Martin J, Maranzana G, Pierfederici S, Weber M, Meibody-Tabar F, et al. Design and modeling of an equalizer for fuel cell energy management systems. IEEE Trans Power Electron 2019:1. https://doi.org/10.1109/TPEL.2019.2899150.

[9] Liu H, Chen J, Hissel D, Lu J, Hou M, Shao Z. Prognostics methods and degradation indexes of proton exchange membrane fuel cells: A review. Renew Sustain Energy Rev 2020;123:109721. https://doi.org/10.1016/j.rser.2020.109721.

[10] Lin RH, Xi XN, Wang PN, Wu BD, Tian SM. Review on hydrogen fuel cell condition monitoring and prediction methods. Int J Hydrogen Energy 2019;44:5488–98. https://doi.org/10.1016/j.ijhydene.2018.09.085.

[11] Zheng Z, Petrone R, Pera M-C, Hissel D, Becherif M, Pianese C, et al. A review on non-model based diagnosis methodologies for PEM fuel cell stacks and systems. Int J Hydrogen Energy 2013;38:8914–26. https://doi.org/10.1016/j.ijhydene.2013.04.007.

[12] Xie R, Ma R, Pu S, Xu L, Zhao D, Huangfu Y. Prognostic for fuel cell based on particle filter and recurrent neural network fusion structure. Energy AI 2020;2:100017. https://doi.org/10.1016/j.egyai.2020.100017.

[13] Kim J, Lee I, Tak Y, Cho BH. State-of-health diagnosis based on hamming neural network using output voltage pattern recognition for a PEM fuel cell. Int J Hydrogen Energy 2011;37:4280–9. https://doi.org/10.1016/j.ijhydene.2011.11.092.

[14] Hissel D, Member S, Candusso D, Harel F. Fuzzy-Clustering Durability Diagnosis of Polymer Electrolyte Fuel Cells Dedicated to Transportation Applications. IEEE Trans Veh Technol 2007;56:2414–20.

[15] Hua J, Li J, Ouyang M, Lu L, Xu L. Proton exchange membrane fuel cell system diagnosis based on the multivariate statistical method. Int J Hydrogen Energy 2011;36:9896–905. https://doi.org/10.1016/j.ijhydene.2011.05.075.

[16] Steiner NY, Hissel D, Mocoteguy P, Candusso D. Non intrusive diagnosis of polymer electrolyte fuel cells by wavelet packet transform. Int J Hydrogen Energy 2010;6:740–6. https://doi.org/10.1016/j.ijhydene.2010.10.033.

[17] Akbaryan F, Bishnoi PR. Fault diagnosis of multivariate systems using pattern recognition and multisensor data analysis technique. Comput Chem Eng 2001;25:1313–39.

[18] Breaz E, Gao F, Miraoui A, Tirnovan R. A Short review Of Aging Mechanism Modeling Of Proton Exchange Membrane Fuel Cell In Transportation Applications. Ind Electron Soc IECON 2014-40th Annu Conf IEEE 2014:3941--3947.

[19] Zhou D, Wu Y, Gao F, Breaz E, Ravey A, Miraoui A, et al. Degradation Prediction of PEM Fuel Cell Stack Based on Multiphysical Aging Model With Particle Filter Approach. IEEE Trans Ind Appl 2016;53:4041–52.

[20] Chen J, Huang L, Yan C, Liu Z. A dynamic scalable segmented model of PEM fuel cell systems with two-phase water flow. Math Comput Simul 2020;167:48–64. https://doi.org/10.1016/j.matcom.2018.05.006.

[21] Qi Y, Espinoza-andaluz M, Thern M, Andersson M. Polymer electrolyte fuel cell system level modelling and simulation of transient behavior. ETransportation 2019;2:100030. https://doi.org/10.1016/j.etran.2019.100030.

[22] Sankar K, Jana AK. Nonlinear multivariable sliding mode control of a reversible PEM fuel cell integrated system. Energy Convers Manag 2018;171:541–65. https://doi.org/10.1016/j.enconman.2018.05.079.

[23] Sankar K, Aguan K, Jana AK. A proton exchange membrane fuel cell with an air fl ow cooling system : Dynamics , validation and nonlinear control. Energy Convers Manag 2019;183:230–40. https://doi.org/10.1016/j.enconman.2018.12.072.

[24] Li Y, Pei P, Ma Z, Ren P, Wu Z, Chen D, et al. Characteristic analysis in lowering current density based on pressure drop for avoiding fl ooding in proton exchange membrane fuel cell. Appl Energy 2019;248:321–9. https://doi.org/10.1016/j.apenergy.2019.04.140.

[25] Ren P, Pei P, Li Y, Wu Z, Chen D, Huang S. Diagnosis of water failures in proton exchange membrane fuel cell with zero-phase ohmic resistance and fixed-low-frequency impedance. Appl Energy 2019;239:785–92. https://doi.org/10.1016/j.apenergy.2019.01.235.

[26] Asensio FJ, Martín JIS, Zamora I, Saldaña G, Oñederra O. Analysis of electrochemical and thermal models and modeling techniques for polymer electrolyte membrane fuel cells. Renew Sustain Energy Rev 2019;113:109283. https://doi.org/10.1016/j.rser.2019.109283.

[27] Petrone R, Zheng Z, Hissel D, Péra M-C, Pianese C, Sorrentino M, et al. A review on model-based diagnosis methodologies for PEMFCs. Int J Hydrogen Energy 2013;38:7077–91. https://doi.org/10.1016/j.ijhydene.2013.03.106.

[28] Li Q, Wang T, Li S, Chen W, Liu H, Breaz E, et al. Online extremum seeking-based optimized energy management strategy for hybrid electric tram considering fuel cell degradation. Appl Energy 2021;285. https://doi.org/10.1016/j.apenergy.2021.116505.

[29] Wu X, Xu L, Wang J, Yang D, Li F, Li X. A prognostic-based dynamic optimization strategy for a degraded solid oxide fuel cell. Sustain Energy Technol Assessments 2020;39. https://doi.org/10.1016/j.seta.2020.100682.

[30] Fernandez AMI, Kandidayeni M, Boulon L, Chaoui H. An Adaptive State Machine Based Energy Management Strategy for a Multi-Stack Fuel Cell Hybrid Electric Vehicle. IEEE Trans Veh Technol 2020;69:220–34. https://doi.org/10.1109/TVT.2019.2950558.

[31] Li Q, Yin L, Yang H, Wang T, Qiu Y, Chen W. Multi-Objective Optimization and Data-Driven Constraint Adaptive Predictive Control for Efficient and Stable Operation of PEMFC System. IEEE Trans Ind Electron 2020;0046. https://doi.org/10.1109/TIE.2020.3040662.

[32] Li Q, Yang W, Yin L, Chen W. Real-Time Implementation of Maximum Net Power Strategy Based on Sliding Mode Variable Structure Control for Proton-Exchange Membrane Fuel Cell System. IEEE Trans Transp Electrif 2020;6:288–97. https://doi.org/10.1109/TTE.2020.2970835.

[33] Liu Z, Chen J, Liu H, Yan C, Hou Y, He Q, et al. Anode purge management for hydrogen utilization and stack durability improvement of PEM fuel cell systems. Appl Energy 2020;275:115110. https://doi.org/10.1016/j.apenergy.2020.115110.

[34] Pahon E, Hissel D, Jemei S, Steiner NY. Signal-based diagnostic approach to enhance fuel cell durability. J Power Sources 2021;506:230223. https://doi.org/10.1016/j.jpowsour.2021.230223.

[35] Zhou Y, Ravey A, Péra MC. Multi-mode predictive energy management for fuel cell hybrid electric vehicles using Markov driving pattern recognizer. Appl Energy 2020;258:114057. https://doi.org/10.1016/j.apenergy.2019.114057.

[36] Vichard L, Harel F, Ravey A, Venet P, Hissel D. Degradation prediction of PEM fuel cell based on artificial intelligence. Int J Hydrogen Energy 2020;45:14953–63. https://doi.org/10.1016/j.ijhydene.2020.03.209.

[37] Qiu D, Peng L, Lai X, Ni M, Lehnert W. Mechanical failure and mitigation strategies for the membrane in a proton exchange membrane fuel cell. Renew Sustain Energy Rev 2019;113:109289. https://doi.org/10.1016/j.rser.2019.109289.

[38] Pei P, Wu Z, Li Y, Jia X, Chen D, Huang S. Improved methods to measure hydrogen crossover current in proton exchange membrane fuel cell. Appl Energy 2018;215:338–47. https://doi.org/10.1016/j.apenergy.2018.02.002.

[39] Candusso D, De Bernardinis A, Peera M-C, Harel F, Francois X, Hissel D, et al. Fuel cell operation under degraded working modes and study of diode by-pass circuit dedicated to multi-stack association. Energy Convers Manag 2008;49:880–95. https://doi.org/10.1016/j.enconman.2007.10.007.

[40] Thomas A. Water and heat transfers in a membrane fuel cell:

experimental demonstration of coupling and analysis of mechanisms. 2012.

[41] Thomas A, Maranzana G, Didierjean S, Dillet J, Lottin O. Thermal and water transfer in PEMFCs : Investigating the role of the microporous layer. Int J Hydrogen Energy 2014;39:2649–58. https://doi.org/10.1016/j.ijhydene.2013.11.105.

[42] Liu ZY, Brady BK, Carter RN, Litteer B, Budinski M, Hyun JK, et al. Characterization of carbon corrosion-induced structural damage of PEM fuel cell cathode electrodes caused by local fuel starvation. J Electrochem Soc 2008;155:B979.

[43] Zhou F, Andreasen SJ, Kær SK, Yu D. Analysis of accelerated degradation of a HT-PEM fuel cell caused by cell reversal in fuel starvation condition. Int J Hydrogen Energy 2015;40:2833–9.

[44] Hu J, Sui PC, Kumar S, Djilali N. Modelling and simulations of carbon corrosion during operation of a polymer electrolyte membrane fuel cell. Electrochim Acta 2009;54:5583–92.

[45] Bahrami M. Contribution to the development of a fuel cell management system. Université de Lorraine, 2020.

[46] Maranzana G, Didierjean S, Dillet J, Thomas A, Lottin O. IMPROVED FUEL CELL. Patent n° : WO/2014/060198. 2014.

[47] Maranzana G, Lamibrac A, Dillet J, Abbou S, Didierjean S, Lottin O. Startup (and shutdown) model for polymer electrolyte membrane fuel cells. J Electrochem Soc 2015;162:F694--F706. https://doi.org/10.1149/2.0451507jes.

[48] Vetter R, Schumacher JO. Experimental parameter uncertainty in proton exchange membrane fuel cell modeling. Part I: Scatter in material parameterization. J Power Sources 2019;438:227018.

[49] Wang C. A Study of Membership Functions on Mamdani- Type Fuzzy Inference System for Industrial. 2015.

[50] Kusoglu A, Karlsson AM, Santare MH, Cleghorn S, Johnson WB. Mechanical response of fuel cell membranes subjected to a hygro-thermal cycle. J Power Sources 2006;161:987–96.